Mixing assessment of an industrial anaerobic digestion reactor using CFD

Zamani Abyaneh, Ehsan; Zarghami, Reza; Krühne, Ulrich; Rosinha Grundtvig, Inês P.; Ramin, Pedram; Mostoufi, Navid

Published in:
Renewable Energy

Link to article, DOI:
10.1016/j.renene.2022.04.147

Publication date:
2022

Document Version
Peer reviewed version

Journal Pre-proof

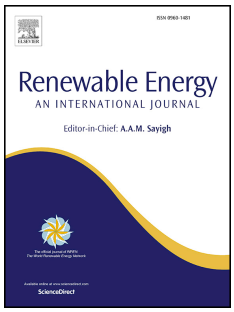

Mixing assessment of an industrial anaerobic digestion reactor using CFD

Ehsan Zamani Abyaneh, Reza Zarghami, Ulrich Krühne, Inês P. Rosinha Grundtvig, Pedram Ramin, Navid Mostoufi

PII: S0960-1481(22)00616-4

DOI: https://doi.org/10.1016/j.renene.2022.04.147

Reference: RENE 17012

To appear in: *Renewable Energy*

Received Date: 21 June 2021

Revised Date: 9 April 2022

Accepted Date: 28 April 2022

Please cite this article as: Zamani Abyaneh E, Zarghami R, Krühne U, Rosinha Grundtvig InêP, Ramin P, Mostoufi N, Mixing assessment of an industrial anaerobic digestion reactor using CFD, *Renewable Energy* (2022), doi: https://doi.org/10.1016/j.renene.2022.04.147.

CRediT author statement

Ehsan Zamani Abyaneh: Writing- Original draft preparation, **Reza Zarghami:** Supervision, **Ulrich Krühne**: Supervision, ***Inês P. Rosinha Grundtvig****:* Visualization, Investigation, **Pedram Ramin**: Validation, Investigation, **Navid Mostoufi:** Supervision, Writing- Reviewing and Editing,

Mixing Assessment of an Industrial Anaerobic Digestion Reactor using CFD

Ehsan Zamani Abyaneh[1], Reza Zarghami[1*], Ulrich Krühne[2], Inês P. Rosinha Grundtvig[2], Pedram Ramin[2], Navid Mostoufi[1]

[1] Process Design and Simulation Research Centre, School of Chemical Engineering, College of Engineering, University of Tehran, P.O. Box 11155/4563, Tehran, Iran

[2] Process and Systems Engineering Center (PROSYS), Department of Chemical and Biochemical Engineering, Technical University of Denmark, Building 229, DK-2800, Kgs. Lyngby, Denmark

Abstract:

A computational fluid dynamic model was developed for an industrial anaerobic digestion reactor to assess its mixing efficiency. The mixing was evaluated by inspecting different parameters, including velocity patterns, dead zones and residence time distribution (RTD). Single-phase simulations were conducted considering and neglecting the presence of solids content and its effect on the viscosity of the slurry. The fluid was considered Newtonian in the absence of solids and non-Newtonian when solids were present. Dead zones were observed in both mixing and expanded sludge bed sections. These zones comprised, respectively, 49volume % and 10volume % of the mixing section and the expanded sludge bed section. The formation of the dead zones can be attributed to inefficiency of the mixing section in pumping flow upward into the middle of the

* Corresponding author: rzarghami@ut.ac.ir

reactor, especially, near the internal circulation pipe. Hence, a modification considering the discussed reasons would be beneficial to avoid the formation of dead zones. In addition, a compartment model representing the RTD is proposed, in which different patterns of plug flow, continuous mixed zones, dead volumes and recycle flow are considered.

Keywords: CFD, Mixing, Anaerobic digestion, dead zone, RTD

1. Introduction

Anaerobic digestion (AD) has received considerable attention in the past decades to reduce pollutants from industrial and agricultural operations. AD has many applications for sludge stabilization and energy recovery and hence can contribute to sustainable operation and energy production in forms of heat and electricity. Attached fixed film, fluidized bed, expanded granular sludge bed (EGSB), upflow anaerobic sludge blanket (UASB) and internal circulation (IC) reactors are the most used high-flowrate systems [1]. This paper investigates the performance of an industrial AD reactor which is a special EGSB with internal circulation.

Designing, benchmarking, diagnosis and optimization of any AD process includes biochemical and physicochemical phenomena. Biochemical phenomena dominate the main steps of the AD process, including hydrolysis, acidogenesis, acetogenesis and methanogenesis (generally the phenomena dealing with microorganisms). Since 1960s, different mathematical models have been developed to correctly describe underlying physic-chemical and biological phenomena. The anaerobic digestion model No. 1 (ADM1) developed by the IWA task group is considered the most comprehensive and widely used AD model [2]. While validating these models against lab-scale

experimental data has been performed with some success [3, 4], validation against full-scale data has been more challenging [5, 6]. This is due to the fact that full-scale digesters do not behave the same as the fully stirred lab-scale systems because of possible formation of stagnation regions and development of concentration, shear stress and temperature gradients inside the reactor. Further complications are also caused by the complex non-Newtonian rheology of the sludge, including shear thinning, shear banding and yield stress [7]. In a non-Newtonian fluid, the viscosity is dependent on temperature, shear rate and even time [8] which can cause inefficient mixing and hence underperforming biogas production. Conventional anaerobic digestion models, such as the ADM1, cannot capture these phenomena as these models are almost exclusively bulk models, assuming uniform property throughout the reactor. These models are also developed largely from the biochemical perspective, and ignore the hydrodynamics [9]. The performance of every AD reactor should be evaluated and improved through considering both biochemical and physicochemical phenomena simultaneously. In an anaerobic digester, the gas yield is largely affected by the retention time inside the reactor (both hydraulic and solids) which is effectively controlled by mixing. Moreover, mixing promotes mass transfer between substrates and active biomass and mass transfer between liquid and the gas phase [10]. This topic is more important since approximately 20% of the total energy consumption of the process is allocated to mixing [11]. Sufficient agitation in an AD reactor prevents the formation of dead zones and provides a uniform environment for maximizing microbial activity and biogas production [12]. Furthermore, precipitation is one of the most prevalent process issues that can be prevented by appropriate mixing [13, 14]. Any improvement in the mixing process would result in lower energy consumption and more biogas yield.

There are several approaches to evaluate the mixing quality. Investigating flow patterns and mixing conditions are traditionally performed using tracer tests to examine the deviations from ideal mixing patterns, locate inactive and short-circuiting zones [15]. Deeper insights to the hydrodynamics of the digester is possible with more advanced methods, including computer automated radioactive particle tracking (CARPT) and computed tomography (CT) [16] as well as positron emission particle tracking (PEPT) [17]. However, these experimental techniques are resource intensive and difficult to apply in full-scale digesters.

Computational fluid dynamics (CFD) has proven to be a promising tool to study the flow fields in a reactor and has been successfully applied for design, redesign and scale up purposes to create optimal mixing conditions [18-20]. Several studies have been conducted to simulate the hydrodynamics of anaerobic digesters [21-24]. In a real-life egg-shaped anaerobic digester, impeller induced mixing combined with pumped recirculation was investigated for different solid concentrations using CFD [25]. Michalopoulos et al. [20] implemented CFD to assess mixing of a pilot-scale periodic anaerobic baffled reactor (PABR). They validated the flexibility of PABR in operating between plug flow and continues stirring conditions. López-Jiménez et al. [26] used CFD methods for different flow conditions. Mixing was analyzed with quantitative and qualitative parameters to understand the effect of geometry on the digester performance. Also, Wu [27] developed a two-stage simulation based on the commercial ANSYS-Fluent software. Dapelo and Bridgeman [13] developed an Euler-Lagrange model applied to a full-scale, biogas-mixed anaerobic digester to investigate improving the mixing efficiency. They also proposed a uniformity coefficient for quantitative evaluation of the mixing quality. Dapelo et al. [28] used the Lattice-Boltzman technique for simulating digesters for the first time and applied Euler–Lagrange

multiphase, non-Newtonian and turbulence modelling jointly with a novel hybrid boundary condition. Table 1 summarizes aims, approach, and principal outcomes of the above-mentioned studies and describes more related studies to this investigation.

Table 1. Summary of aims, approaches and principal outcomes of previous investigations

Authors	**Aim**	**Approach**	**Outcome**
Karama et al. [21]	Simulation of an activated sludge reactor	CFD, RTD experiments, Dead zone evaluation	Improving hydraulic flow
Peplinski et al. [23]	Simulation of a full-scale reactor	CFD, Uncertainty analysis based on the RTD curve	RTD was more sensitive to uncertainty in turbulence
Meister et al. [25]	Simulation of Newtonian & Non-Newtonian flows in an egg-shaped anaerobic digester	CFD, Multiple reference frame method, Grid convergence index	Comparison of turbulence models, proposing the efficient rotation speed
Michalopoulos et al. [20]	Hydraulic behavior of a periodic anaerobic baffled reactor	Experimental and numerical (CFD) assessment, RTD experiments, Tanks in series model, Dead zone evaluation	Plug flow and mixed flow condition comparison, comparison of different HRT/T values
López-Jiménez et al. [26]	Hydraulic flow assessment	CFD, Dead zone evaluation	Proposing configurations to prevent dead zone formation
Wu [27]	Integration of mixing, heat transfer, and biochemical kinetics in anaerobic fermentation	Two-stage simulation including CFD and Runge–Kutta method, Comparison between egg-shaped and plug flow digesters	Relating temperature, bacterial grows, residence time distribution and pH to each other
Huang et al. [29]	Considering hydraulic flows while implementing ADM1 model	Lithium tracer experiments, Increasing-size continuous stirred tank reactors (ISC) model, Equal-sized CSTRs (ESC) model, Extended equal-sized CSTRs (EESC) model	Validating results of models with experimental data
Dapelo et al. [14]	Euler-Lagrange simulation	CFD simulation, Particle image velocimetry (PIV), Shear rate assessment, GCI assessment	Validating the model against lab-scale data, unveiling importance of GCI tests
Dapelo and Bridgeman [13]	Euler-Lagrange simulation of a full-scale digester	CFD, Uniformity assessment, Dead volume evaluation, Different rheology consideration	Encouraging usage of uniformity index and non-Newtonian rheology for simulating sludge
Dapelo et al. [28]	Utilizing a novel Lattice-Boltzmann model	Homogenized Lattice Boltzmann model (HLBM), PIV measurements, Partial slip boundary condition	Utilizing the model and validating against experimental work, Providing the chance to simulate biokinetics and hydrodynamics together

CFD provides detailed flow field characteristics of a non-homogenized reactor, but there exist less computationally demanding and simplified approaches to describe non-ideal mixing conditions in a reactor. This has been done by compartmentalization of the reactor, establishing back mixing flow between compartments and bypass streams, as several configurations were suggested for up flow anaerobic sludge blanket (UASB) [9]. A serial tank approach was also adopted by Huang et al. [29] to describe the ADM1 together with hydrodynamics in a lab-scale internal circulation anaerobic reactor.

The objective of this study is to exploit CFD to evaluate the mixing conditions in an industrial scale anaerobic digestion reactor by determining the velocity distribution, formation of dead zones and RTD. To evaluate the deviation of flow patterns from ideal behavior, a non-Newtonian model was compared with a Newtonian model. Furthermore, different simplified modelling approaches were investigated for less computationally demanding simulations. These models were extended equally-sized CSTRs, increasing-sized CSRTs and a compartment model.

2. Model Development

2.1. Digester Configuration

The considered digestion reactor in this investigation is shown in Figure 1. It has a volume of more than 2100 m^3 and it is more than 30 m in height. The reactor operates at a constant temperature of 35 ºC (mesophilic conditions) and consists of four main sections: I) mixing, II) expanded sludge bed, III) polishing and IV) gas-liquid separator. Influent enters the mixing section through several nozzles to achieve an even distribution of the feed. After the mixing region, the sludge flows to the expanded sludge bed, where most of the organic pollutants are converted into biogas. The

biogas is collected in the lower part of the separation module and water flows upward to the polishing section, where the rest of the organic matter is converted into biogas. The gas production rate in this section is less than that in the expanded bed due to a lower concentration of organic matter. Consequently, only the mixing and expanded sludge bed sections were simulated in this study. Finally, the fluid flows to the gas-liquid separator. In this section, water and biogas are separated and water is recycled into the mixing section (internal circulation).

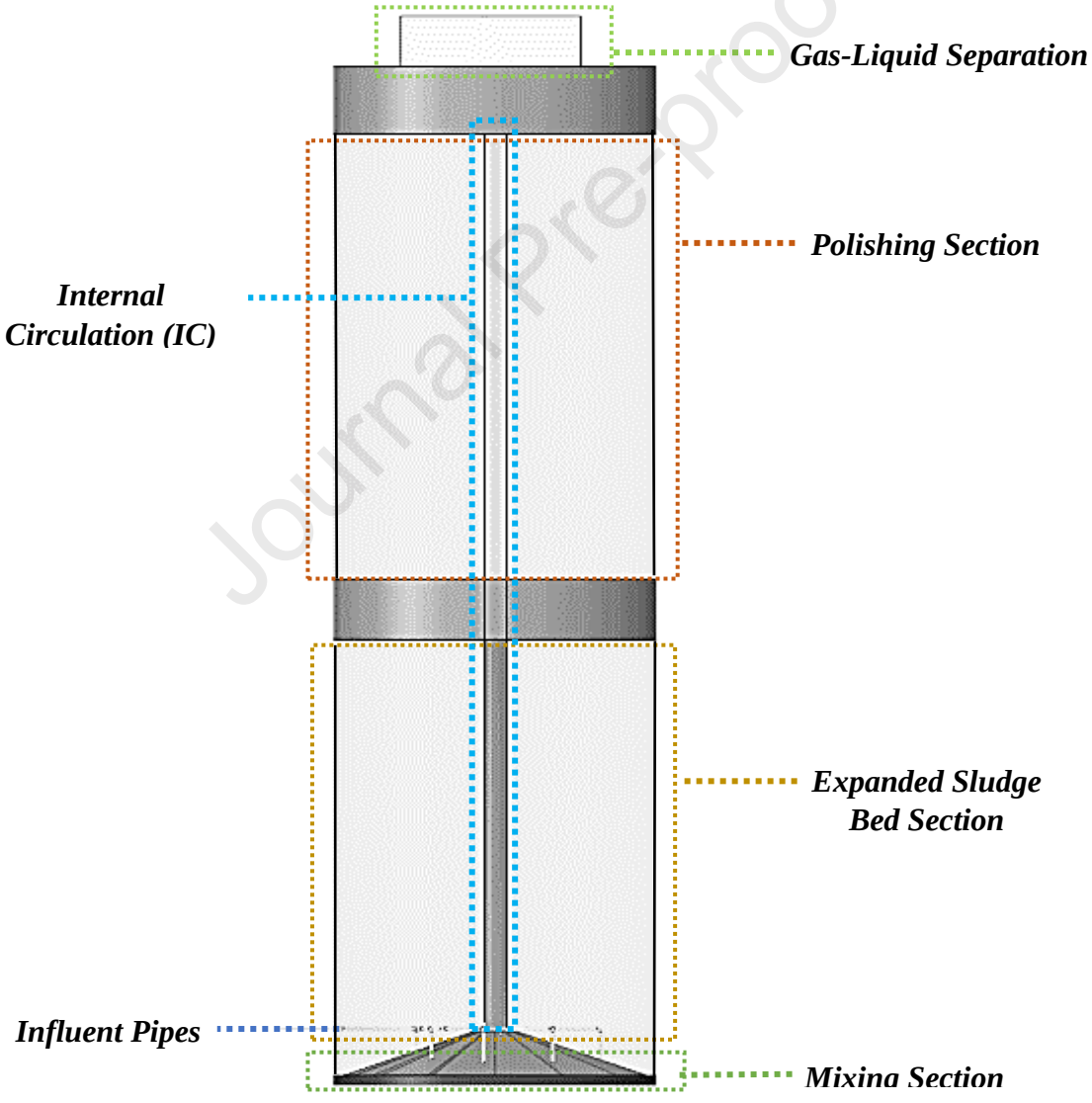

Figure 1. Reactor configuration

2.2. Meshing

The geometries of the mixing and expanded sludge bed sections were generated by Spaceclaim and four meshes were constructed by the ANSYS meshing software in different sizes. The quality of all meshes were validated with a skewness, aspect ratio and element quality analysis. Table 2 represents the average values for every quality scale in each grid size. Mesh elements have a significant impact on simulation results in some areas. When the mixture of influent and recycled flow exits the mixing section, mesh cells on the output surfaces are of great importance. Therefore, mesh refinement was utilized to ensure a qualified mesh in these areas. As shown in Figure 2, proximity and curvature methods were used in generating meshes in both mixing and expanded sludge bed sections. Furthermore, grids were generated in a structured pattern in the expanded sludge bed section. Inflation layers on the reactor wall properly consider the angular velocity in the reactor and fine elements near the internal circulation pipe take into account the wall functions efficiently. Due to the complex configuration and multiplicity of components in the mixing section, an unstructured mesh using triangular elements was generated in this section.

Table 2. Mesh characteristics

Id	Number of cells	Average skewness	Average aspect ratio	Min. volume (m^3)	Max. volume (m^3)	Average element quality
Grid 1	1,314,933	0.257	1.900	1.23×10^{-7}	0.031	0.819
Grid 2	1,482,182	0.248	1.879	9.89×10^{-7}	0.030	0.826
Grid 3	1,929,204	0.256	1.902	3.84×10^{-8}	0.030	0.819
Grid 4	3,703,982	0.229	2.055	3.331×10^{-8}	0.009	0.791

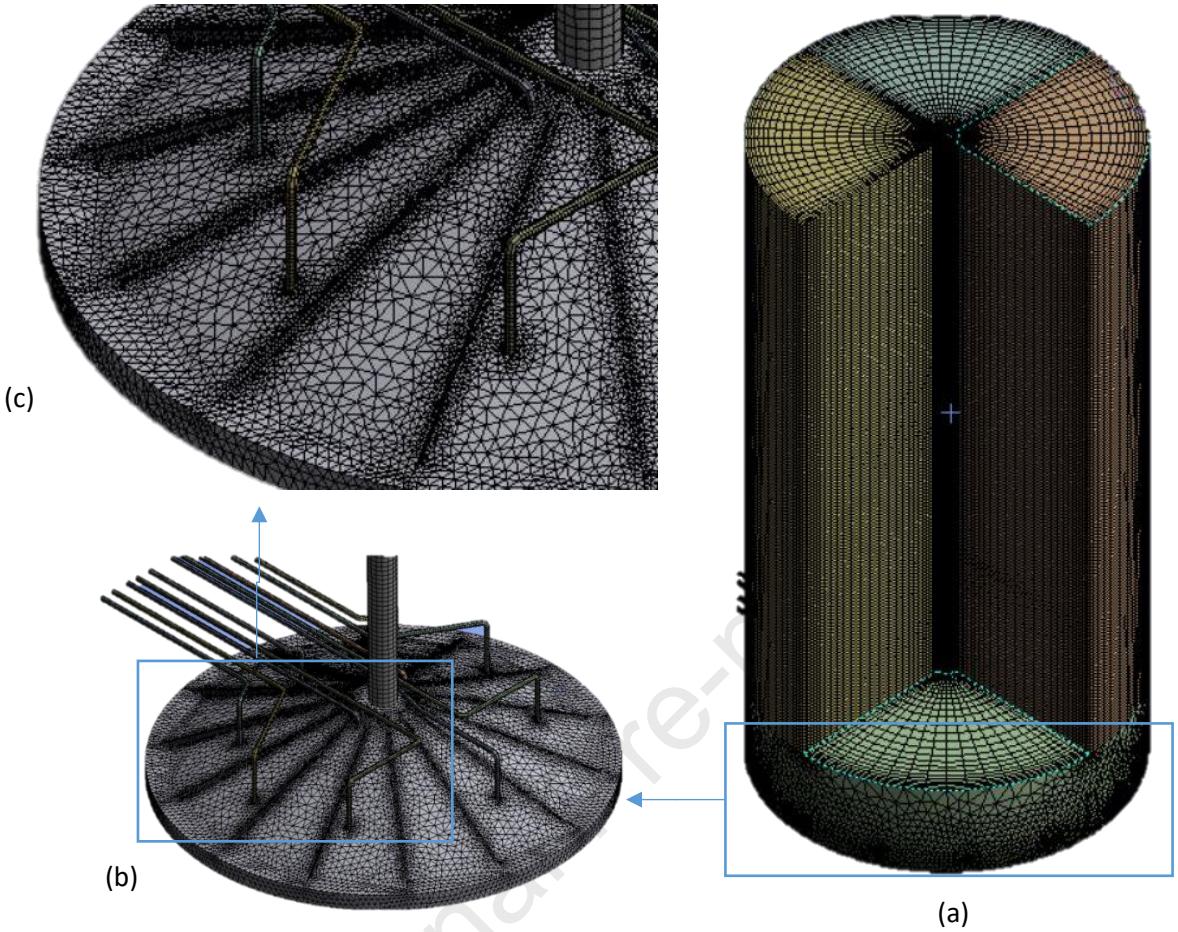

Figure 2. Grid overview (a) expanded sludge bed section (b) mixing section (c) mixing section with higher resolution

2.3. Computational Fluid Dynamics Modeling

Due to the large volume of the reactor and thus high calculation expenses, only the mixing and expanded sludge bed sections were simulated in this study. Such a consideration is reasonable since the aim of this study was to investigate the hydrodynamics, especially the mixing, in this digester. Moreover, the conversion takes place mostly in the expanded bed section.

Simulations were carried out for a single liquid phase under turbulent flow conditions and considering a three-dimensional configuration. The governing equations consist of the continuity and momentum equations:

$$\nabla \cdot \vec{u} = 0 \tag{1}$$

$$\frac{\partial}{\partial t}(\vec{u}) + \nabla \cdot (\vec{u}\vec{u}) = \frac{1}{\rho}(-\nabla \mathrm{p} + \nabla\tau + \rho\vec{g}) \tag{2}$$

Dapelo et al. [30] used the Reynolds stress model for reproducing the turbulent flow of the liquid around the bubbles. Among the large number of turbulence models, the two-equation models (i.e., standard *k*-ε, realizable *k*-ε and *k*-ω) have been widely used and validated against experimental data [25, 26, 31-33]. Since there is no rotational structure in this study, the standard *k*-ε turbulence model was considered appropriate for this work [34]. The transport equations for turbulence kinetic energy (*k*) and its dissipation rate (ε) are as follows:

$$\frac{\partial k}{\partial t} + \nabla \cdot (k\vec{u}) = \frac{1}{\rho}\left(\nabla \cdot \left[\left(\mu + \frac{\mu_t}{\sigma_k}\right)\nabla \mathrm{k}\right] + G_k + G_b - \rho\varepsilon\right) \tag{3}$$

$$\frac{\partial \varepsilon}{\partial t} + \nabla \cdot (\varepsilon\vec{u}) = \frac{1}{\rho}\left(\nabla \cdot \left[\left(\mu + \frac{\mu_t}{\sigma_\varepsilon}\right)\nabla\varepsilon\right] + C_{1\varepsilon}\frac{\varepsilon}{k} + (G_k + C_{3\varepsilon}G_b) + C_{2\varepsilon}\rho\frac{\varepsilon^2}{k}\right) \tag{4}$$

The turbulent (or eddy) viscosity (μ_t) was computed from:

$$\mu_t = \rho_m C_\mu \frac{k^2}{\varepsilon} \tag{5}$$

where ρ is the liquid density, $\vec{u}$ is the velocity, p is the static pressure, τ is the viscous stress, k is the turbulence kinetic energy, G_k is the generation of turbulence kinetic energy due to the mean velocity gradients, G_b is the generation of turbulence kinetic energy due to buoyancy, ε is the specific dissipation rate and $C_{1\varepsilon}$, $C_{2\varepsilon}$ and $C_{3\varepsilon}$ are constants. σ_k and σ_ε are the turbulent Prandtl numbers for the k and ε, respectively. Simulations were performed using the commercial software ANSYS Fluent 19. They were executed using the transient mode and adaptive time steps as well

as the semi-implicit method for pressure linked equations (SIMPLE) scheme. Also, quadratic upstream interpolation for convective kinematics (QUICK) spatial discretization was applied [30]. A hybrid initialization was utilized for the initial conditions and each run continued until reaching the steady-state. The steady-state condition was considered reached when the velocity vectors did not change noticeably against time. Residuals were set at 1×10^{-4} and the computation times for different cases were between 4 to 21 days on a 12-core Intel (R) core ™ i7*5820k CPU 3.3 GHz computer. No-slip conditions were considered for all walls. Influent pipes and internal circulation pipe flowrates were defined as inlets with specified velocity. In real operation conditions, influent flowrates fluctuate and it may increase up to 300 m^3 hr^{-1} in some cases. We used an average flowrate and assumed it to be constant. The outlet, at the top of the expanded sludge bed section, was defined as the outflow.

2.5. Sludge Rheology

In a number of research studies, the sludge was considered as a Newtonian fluid [35, 36]. However, the presence of solids in the sludge makes it a non-Newtonian fluid, which provides different results. The Herschel-Bulkley model was considered as the non-Newtonian model in this work as suggested by other investigations [37, 38]. The shear stress in this model is defined as:

$$\tau = \tau_0 + K|\dot{\gamma}|^n \quad (6)$$

where τ_0 is the critical stress, K is the consistency coefficient and $\dot{\gamma}$ is the strain rate. An important parameter, which affects the rheological model constants is the presence of suspended solids. The rheological constants of the sludge are given in Table 3 for both the Hershel-Bulkley and the Newtonian fluids respectively, adopted based on other researchers' studies [13, 39]. Total suspended solids (TSS) in the reactor were measured for data sets 1 and 2 reported in [40] and the

192 strain rate determined in the range of 0.15-11.51 s^{-1} by performing simulations. The Newtonian
193 model can be considered as a limiting case in simulations of this work, which resembles meager
194 solid contents. In fact, the presence of solid particles causes a deviation of the rheology and making
195 the behavior of the fluid Non-Newtonian. Therefore, according to neglecting and considering the
196 effect of the solid content, Newtonian and non-Newtonian methods were used in this work as the
197 ideal and the real cases, respectively. Figure 3 represents the shear stress against the strain rate for
198 Newtonian and non-Newtonian models for sludge using the coefficients presented in Table 3.
199

200 Table 3. Rheological properties of the sludge for different TSS and $\dot{\gamma}$ ranges

Model	TSS (wt %)	τ_0 (Pa)	K (Pa s^n)	n (-)	$\dot{\gamma}$ range (s^{-1})
Non-Newtonian [7]	**1.85**	**0.092**	**0.169**	**0.308**	**0.01-30**
Newtonian [7]	**-**	**0**	**12**	**1**	**-**

201

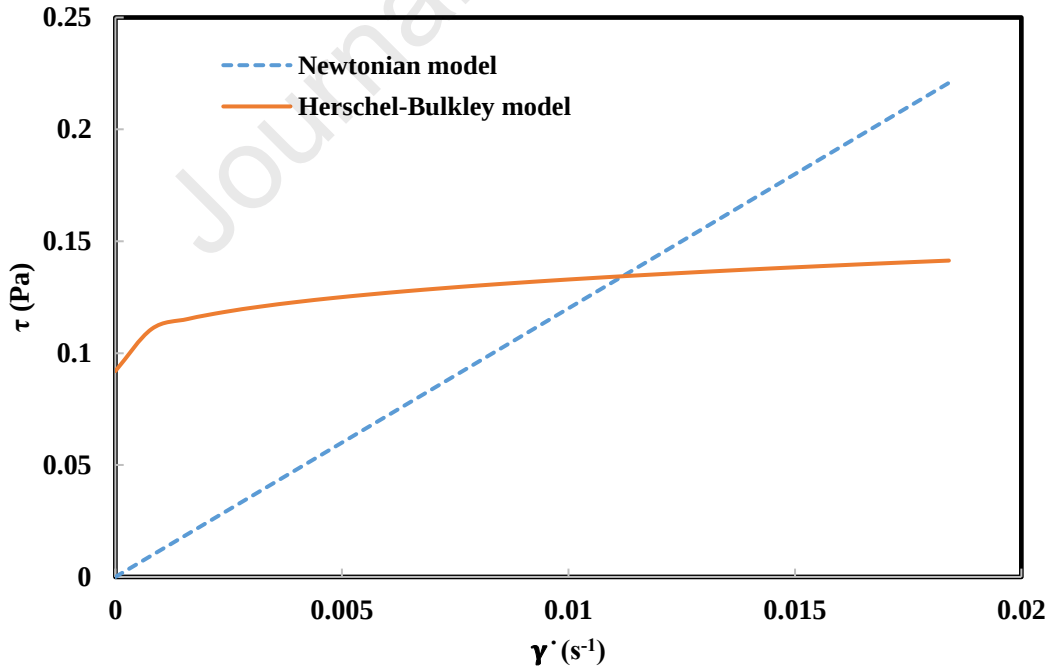

202

Figure 3. Rheological properties of the sludge for different TSS and $\dot{\gamma}$ ranges, adopted from [13, 39]

2.6. Residence Time Distribution

The residence time is a measure of how long the fluid stays in a system for continuous flow reactors and is used for the hydrodynamic characterization. In this study, the pulse method was employed to evaluate the RTD by performing tracer simulations. The tracer was considered as a non-reactant material with the same properties as the main fluid and injected for 0.5 seconds at the reactor inlet. The plot of tracer concentration versus time at the outlet of the reactor was used to determine the RTD, $E(t)$ and mean residence time ($\bar{t}$):

$$E(t) = \frac{C(t)}{\int_0^\infty C(t)dt} \tag{7}$$

$$\bar{t} = \frac{\int_0^\infty t\, E(t)dt}{\int_0^\infty E(t)dt} \tag{8}$$

where $C(t)$ is the tracer concentration at time t. To compare systems with different mean residence times, the normalized time (θ) and the exit-age function, $E(\theta)$, are used and calculated as follows:

$$\theta = \frac{t}{\bar{t}} \tag{9}$$

$$E(\theta) = \bar{t}E(t) \tag{10}$$

2.7. Serial Tank Model

A serial model of tanks can also be used for describing the RTD curve. Advantages of this model are the simplicity and the opportunity to include reaction kinetics. The variance distribution of the RTD (σ_t^2) and the dimensionless variance can be calculated as follows:

$$\sigma_t{}^2 = \frac{\int_0^\infty \left(t-\bar{t}\right)^2 E(t)dt}{\int_0^\infty E(t)dt} = \int_0^\infty t^2 E(t)dt - \left(\bar{t}\right)^2 \quad (11)$$

220 The dimensionless variance is defined as [42]:

$$\sigma_\theta{}^2 = \frac{\sigma_t{}^2}{\bar{t}^2} \quad (12)$$

221 Dimensionless RTD and variances of serial tank model can be summarized as:

$$E(\theta) = (N\bar{t_i})E = N\frac{(N\theta)^{N-1}}{(N-I)!}e^{-N\theta} \quad (13)$$

222 where *N* is the number of equally-sized CSTRs (ESC) which can be calculated as follows:

$$N = \frac{1}{\sigma_\theta{}^2} \quad (14)$$

223 When *N* is not an integer number, it should be rounded to the nearest integer number. Otherwise,
224 we can use the extended equal-sized CSTRs model (EESC) with non-integer *N* values utilizing the
225 Gamma distribution (*Γ*).

$$E(\theta) = \frac{N^N}{\Gamma(N)}\,\theta^{N-1}e^{-N\theta} \quad (15)$$

226

227 Another model which has been a useful utility in recent studies [29, 43] is the increasing-sized
228 CSRTs model (ISC). The performance of this model can be expressed as below:

$$E(\theta) = \sum_{i=1}^{N} \frac{r_i{}^{N-2}}{\prod_{j=1,j\neq i}^{N}(r_i + r_j)}\, e^{-\frac{\theta}{r_i}} \begin{cases} r_i + r_2 + \cdots + r_N = 1 \\ \dfrac{r_k}{r_{k-1}} > 1 \\ 2 \le k \le N \end{cases} \quad (16)$$

229 where r_i is the volume fraction coefficient and *N* is the number of tanks.

230

231 **2.8. Compartment Model**

Compartment models simplify different levels of sophistication for different flow models. In this method, every vessel will be considered by a combination of ideal compartments such as plug flow or mixed flow. Furthermore, every stream will be described by active flow (within the plug or mixed vessels), bypass flow or recycle flows [42]. By comparing the $E(t)$ curves of a combination of ideal cases with the real vessel E curve, the best compartment model, which fits the existence results, can be determined. Figure 4 shows the most similar model to case in this work. This compartment mode includes plug flow, dead volume and well-mixed vessels and a recycle stream. Volumes of each component are determined in the results section. In this study, the well-mixed component was considered as the serial CSTRs with increasing volumes. The dead zone is not a part of plug flow only and is attributed to the whole system.

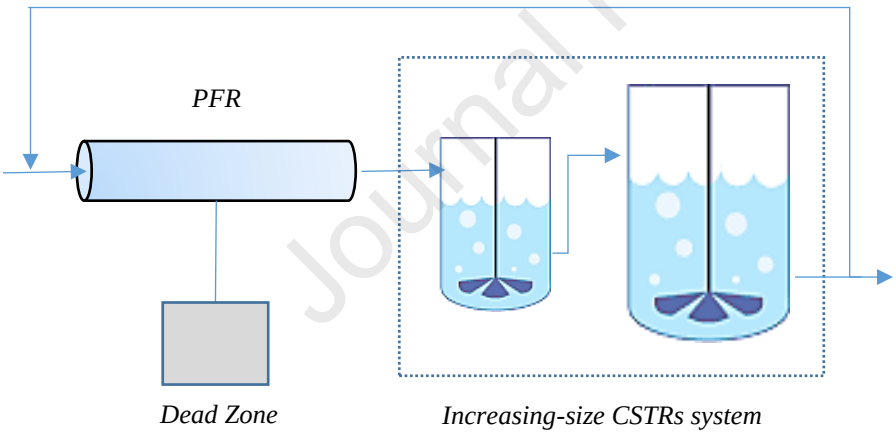

Figure 4. Proposed compartment model

The performance of increasing volume CSTRs can be expressed as:

$$E(t) = \frac{1}{\tau_1} e^{\frac{-t}{\tau_1}} + \frac{1}{\tau_2} e^{\frac{-t}{\tau_2}} - \left(\frac{1}{\tau_1} + \frac{1}{\tau_2}\right) e^{\left(\frac{t}{\tau_1} + \frac{t}{\tau_2}\right)} \quad (17)$$

where τ_1 and τ_2 are the residence times of reactors. The performance of the whole compartment model has a time lag in comparison with the increasing volume CSTRs. This time lag is represented by a PFR. The time lag is the residence time of the plug flow component and can be calculated as:

$$\tau_P = \frac{V_p}{\upsilon} \tag{18}$$

where V_p is the volume of the plug flow reactor and υ is the volumetric flowrate entering the system.

3. Results and Discussion

Simulations were checked for grid-independency by measuring dead volume and velocity average within the reactor and calculating the grid convergence index (GCI) [44]. Description of this method is given by Dapelo et al. [14]. Table 4 shows the calculated GCIs. Based on the results shown in this, grids 2, 3, and 4 have reached convergence based on the asymptotic range, while grid 1 falls outside of this range. Therefore, grid 3 with 1,929,204 elements was selected for performing the simulations of this work.

Table 4. GCI calculations

	Average Velocity (m.s^{-1})		**Dead volume**	
	Non-Newtonian	**Newtonian**	**Non-Newtonian**	**Newtonian**
Grid 1	0.0185	0.019	0.0825	0.0445
Grid 2	0.018	0.024	0.0751	0.0428
Grid 3	0.0175	0.022	0.0712	0.0352
Grid 4	0.0178	0.03	0.0724	0.0377
P_1	4.34	5.9	9.84	1.30
P_2	1.26	2.56	3.57	3.3
$GCI2_{43}$	0.0232	0.4940	0.0229	0.0965
$GCI2_{32}$	0.1184	0.3767	0.2270	0.8948
$GCI1_{32}$	0.1151	0.3453	0.2152	0.7359
$GCI1_{21}$	0.2729	2.0474	0.9683	0.3903
Asymp 1	0.7553	1.2516	0.3362	0.3765

Asymp 2	1.042	1.11604	0.9657	1.0773

3.1. Flow Patterns Investigation

3.1.1. Non-Newtonian Model

Figure 5 shows the evolution of velocity contours after feed injection in the mixing section. The solid content in the influents is 2.35% for which the mixture follows the Herschel-Bulkley rheological model. The flow reaches steady-state in about 6000s and an axial dispersion flow pattern forms gradually close to the reactor wall. However, no significant transient radial velocity gradient is formed and a significant decrease in the velocity is observable in the radial direction from the reactor wall toward the internal circulation pipe.

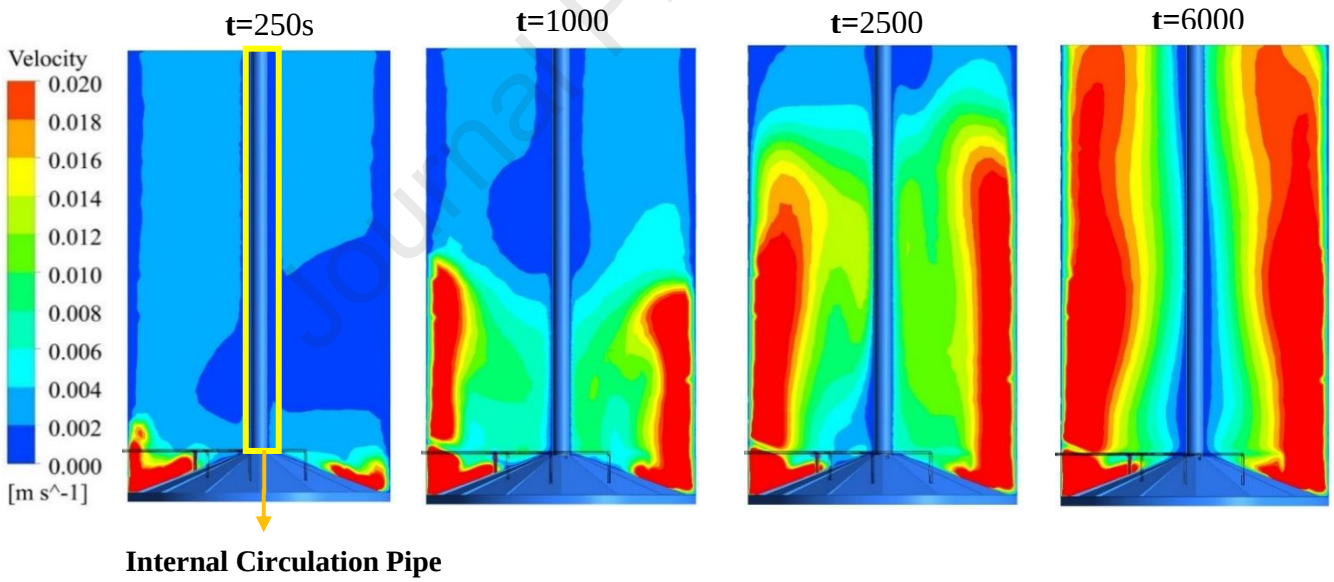

Figure 5. Contours of velocity magnitude at various times after injection of feed in non-Newtonian fluid simulation

277 Figure 6 demonstrates the velocity magnitude vectors in the expanded sludge bed section after
278 reaching the steady-state conditions. Fluid exits from the mixing section through the output
279 surfaces and enters the expanded sludge bed section. The way that fluid exits from these surfaces
280 and the tangential injection of feed at the mixing section, forms an angular velocity and axial
281 dispersion in the expanded sludge bed section, which promotes agitation in this section. In
282 addition, the exit flow through the output surfaces is not uniform and near the center almost no
283 flow can be detected. Such a pattern results in a lack of agitation and leads to dead zones formation
284 near the internal circulation pipe.

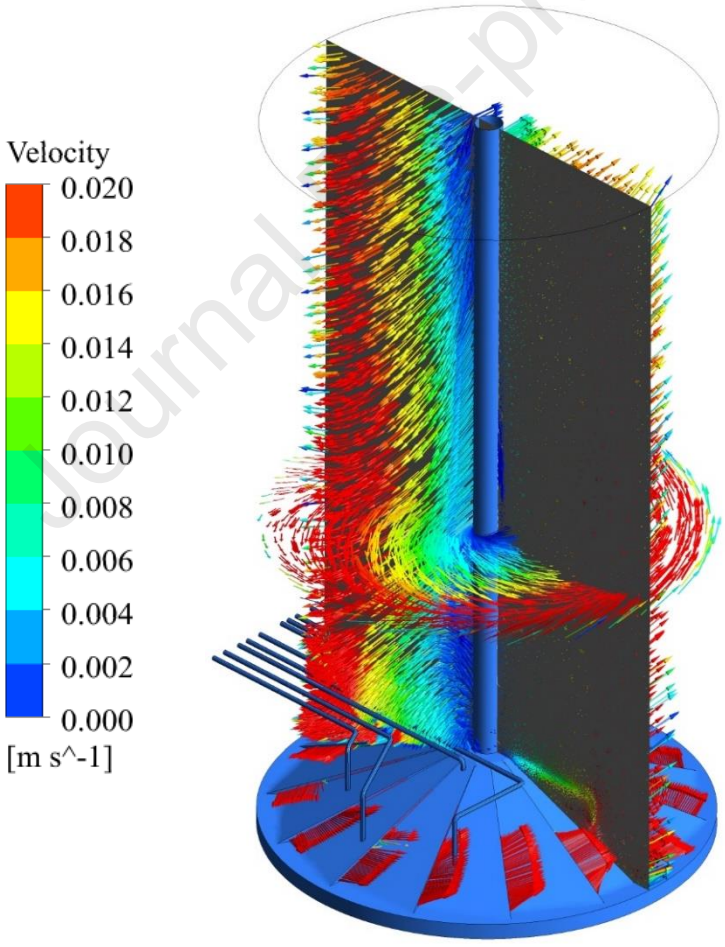

285

286 Figure 6. Velocity vectors in the expanded sludge bed section for the non-Newtonian fluid at the
287 steady-state condition

3.1.2. Newtonian Model

The modelling of the liquid with Newtonian properties can be considered as a liming condition for very diluted sludge. Figure 7 presents the velocity contour plot and velocity vectors for steady-state conditions for such fluid simulation with very diluted sludge. Comparing this figure with those for the non-Newtonian case reveals a greater radial velocity gradient in the Newtonian fluid. Such higher velocity gradients result in a more intense downward flow near the internal circulation pipe in the middle of the expanded sludge bed which creates an axial circulation within this section. This difference can be attributed to the critical shear stress in the non-Newtonian model as a result of solid particles which makes the mixture to show greater resistance against motion. The higher average velocity in the Newtonian fluid results in a better agitation, which reduces the time for reaching the steady-state condition to 1500s (compared to 6000 s for non-Newtonian). The higher velocity generates a larger vortex (discussed later) in the middle of the expanded sludge bed section. This vortex promotes the downward flow near the internal circulation pipe and generates the axial circulation.

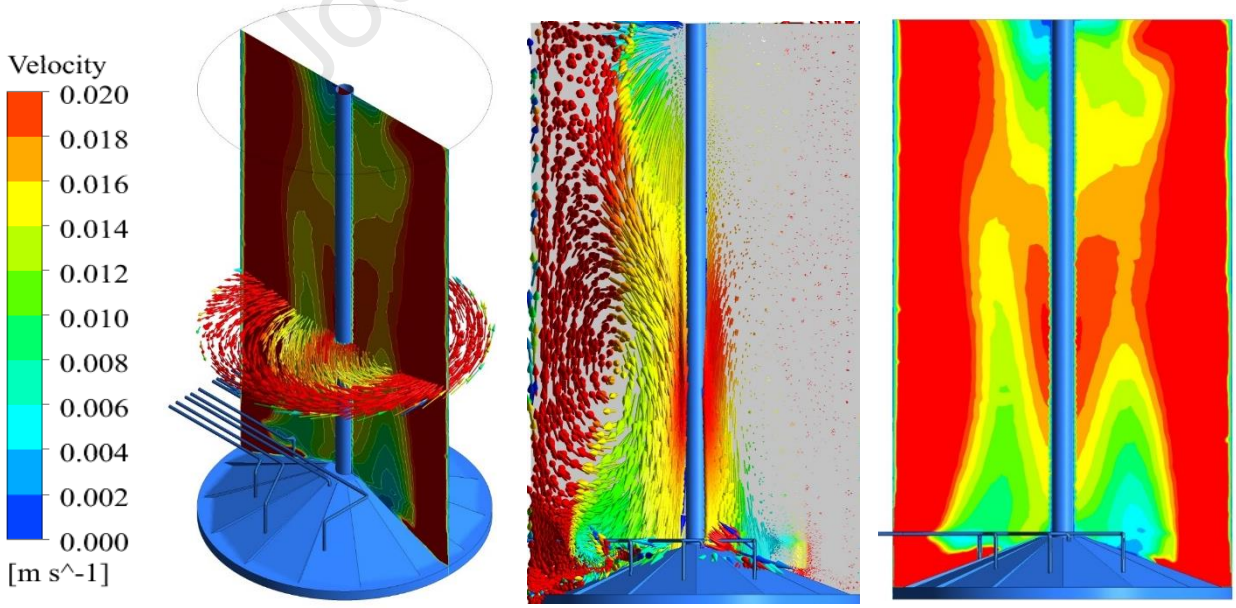

(a) (b) (c)

Figure 7. Simulation results for the Newtonian fluid at the steady-state condition: (a) vectors of angular velocity. (b) vector of axial velocity. (c) velocity magnitude field

3.2. Dead Zones

Deviation from ideal flow patterns can be caused by channeling, recycling or formation of dead regions. There are different ways to specify dead zones. As a simple and basic definition, dead zone is considered as a part of the reactor in which the velocity is less than 5% of the maximum fluid velocity in the reactor [35, 45]. More complex and pioneer way to specify dead zones is developed by Dapelo et al. [13] by presenting uniformity coefficient approach. Dead zones can also be generated by vortexes and creating semi-stagnant zones [35, 46]. Dead zone is considered as a cut off from the surrounding flow and its formation should be avoided because it reduces the reactor performance. Consequently, influent sludge would be unable to reach the dead zone and almost no reaction takes place in this area [13, 46]. A dead zone evaluation in this study was carried out for the real fluid properties of the non-Newtonian rheological model. However, the comparison is also made with the Newtonian fluid limit case.

Figure 8 shows the velocity vectors in the mixing and expanded sludge bed sections for the non-Newtonian fluid that follows the Herschel-Bulkley model. Formation of dead zones near the internal circulation pipe and disturbance of influent pipes are shown in this figure. Figure 8a illustrates dead zones near the internal circulation pipe. These dead areas are formed as a result of a strong upward flow far from and weak downward flow near the internal circulation pipe. The formation of these dead zones can also be attributed to the mixing section inefficiency in producing agitation in the middle of the sludge bed section. Figure 9b shows that strong vortices are generated

326 in the middle of the mixing section. These vortices are formed due to intensive downward flow by
327 the internal circulation pipe. This section does not work properly and cannot pump the fluid in the
328 axial direction through the expanded sludge bed section. In addition, the tangential injection of
329 influents leads to less agitation in the middle of this section. Another noticeable phenomenon
330 presented in Figure 8 is the formation of local vortices in the expanded sludge bed section. These
331 vortices can be useful and provide better mixing and agitation.
332

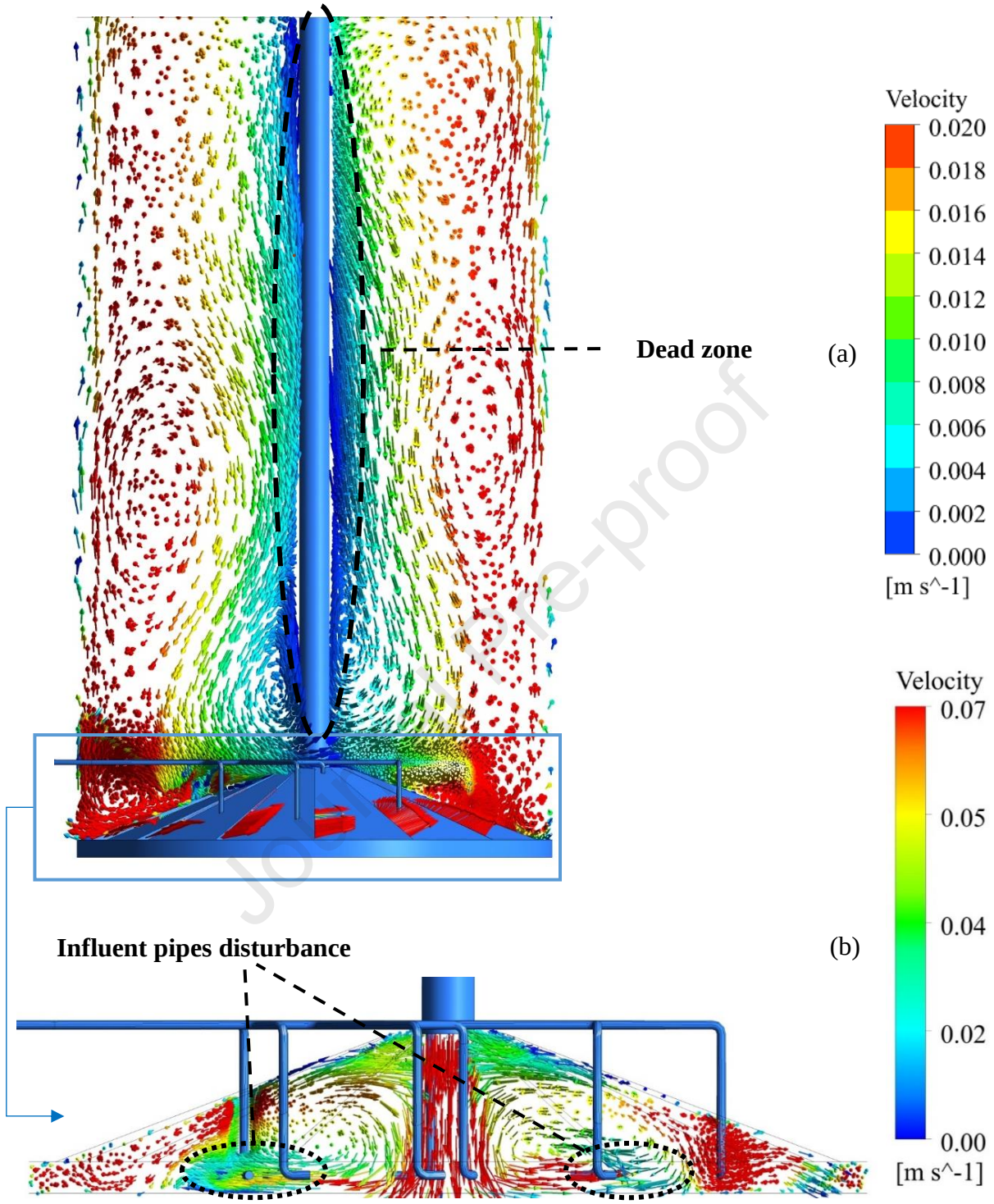

Figure 8. Side view of the velocity vectors in mixing and expanded sludge bed sections for the non-Newtonian fluid simulation: (a) Expanded sludge bed and mixing section (b) Mixing section

Figure 9 shows velocity vectors exiting from the mixing section for the non-Newtonian fluid that uses the Herschel-Bulkley model. There is no considerable outflow at upper portions of the mixing section. As discussed above, the main reason of this pattern is inefficient pumping flow from the middle of the mixing section and tangential injection of influent pipes. Such a pattern helps the creation of dead zones near the internal circulation pipe in the expanded sludge bed section shown in Figure 6.

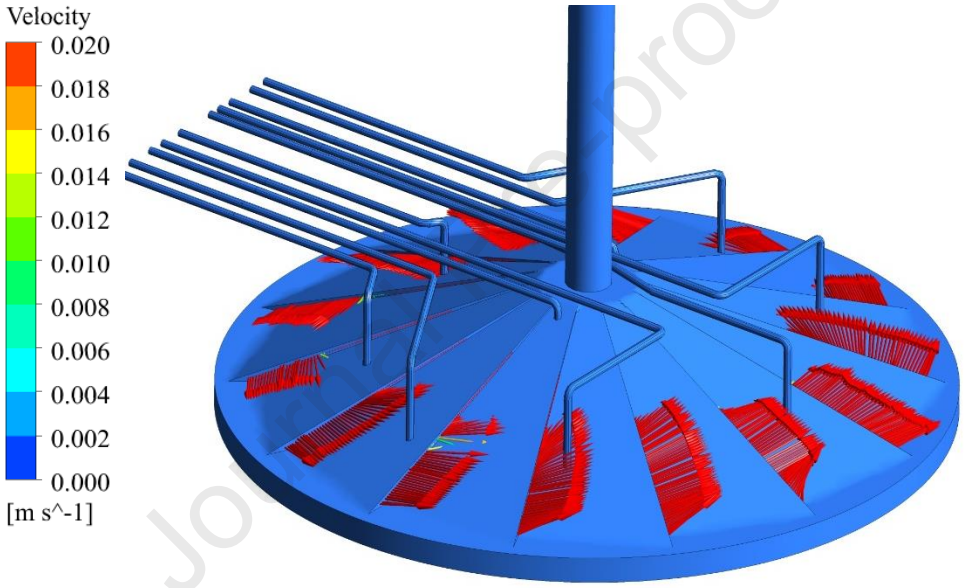

Figure 9. Velocity vectors exiting from the flow output surfaces in the non-Newtonian fluid simulation

Figure 10 shows the dead volumes in the mixing and expanded sludge bed sections for the non-Newtonian fluid simulation. The colored volumes represent the dead zones and depict the areas that have a velocity less than 5% of the maximum fluid velocity in the reactor. Dead areas formed near the internal circulation pipe in the expanded sludge bed section are presented in Figure 10a. These dead zones are extended from above the mixing section up to the end of the expanded sludge

353 bed section. Figures 10b and 10c are two views of mixing section dead zones. The dead zones in
354 the middle of the mixing section are noticeable. These figures also reveal that in spite of a
355 tangential injection of influents, some dead volumes are formed at the wall of the mixing section.

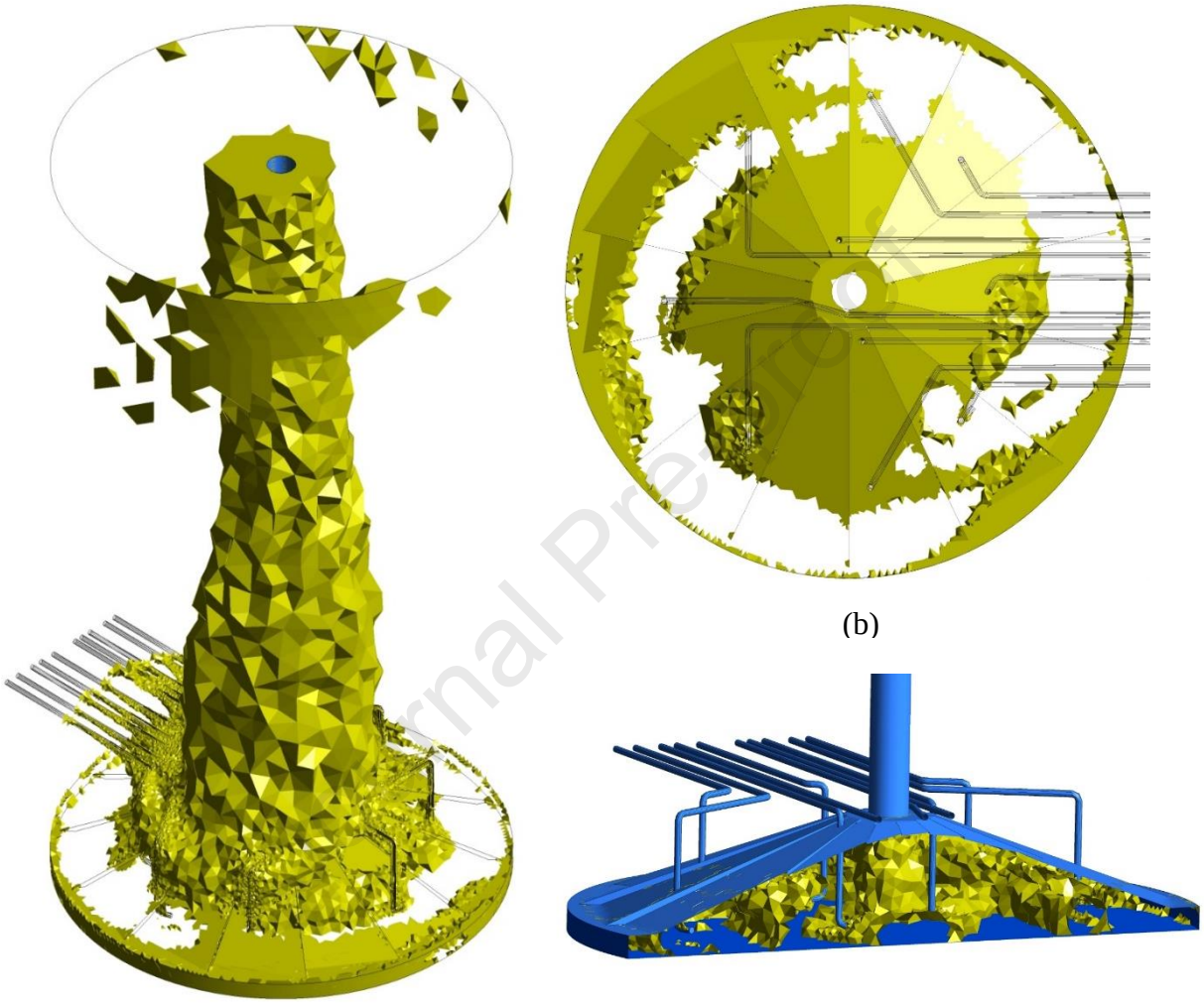

(a) (b) (c)

356

357 Figure 10. Dead zones in non-Newtonian simulation: (a) Mixing and expanded sludge bed
358 sections (b) Mixing section from above (c) A slice of the mixing section

359

360 Figure 11 presents the lateral view of the velocity field in both the mixing and expanded sludge
361 bed sections for the Newtonian fluid simulation. Axial circulation is visible in this figure. The axial

362 circulation has been formed on the internal circulation pipe and it can prevent dead zone formation
363 near this pipe in the expanded sludge bed section. Like the non-Newtonian simulations, some local
364 vortices can be detected in this simulation. It is worth noting that they are more in number and
365 greater in intensity compared with the non-Newtonian case.
366

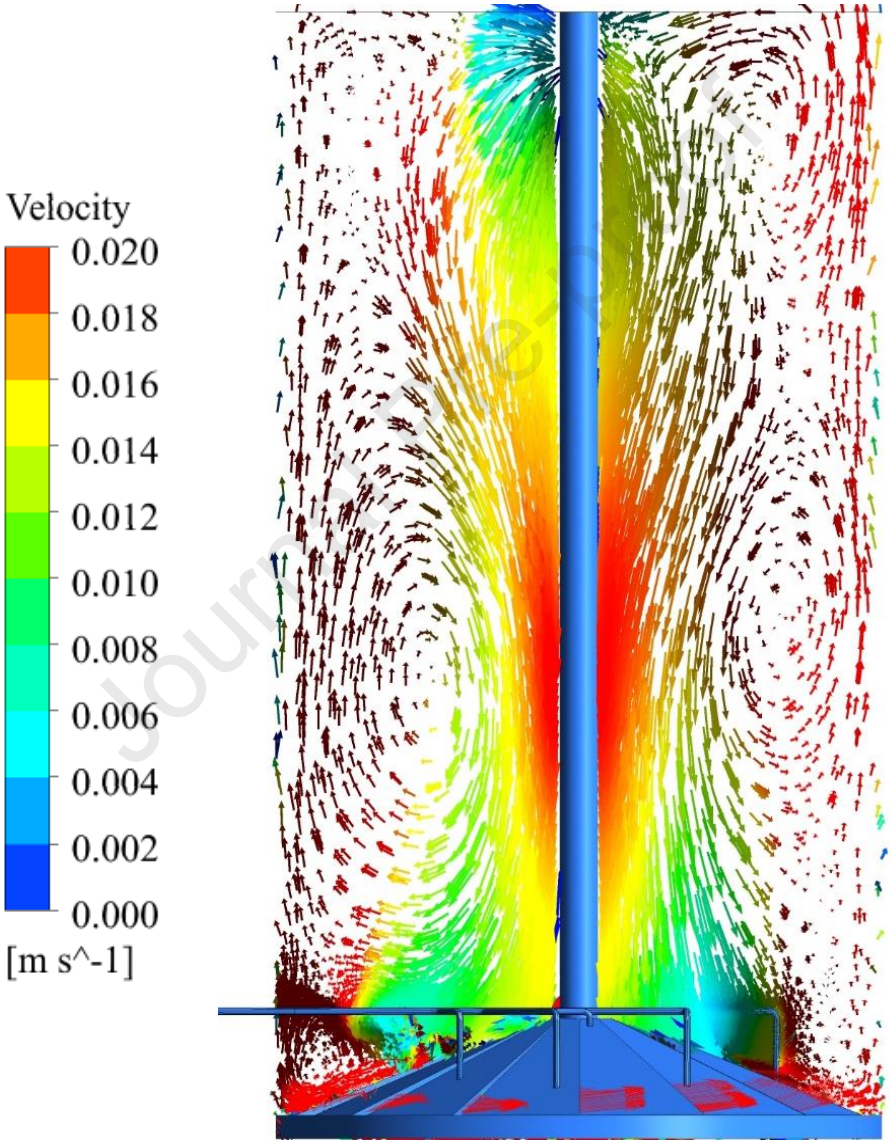

367

368 Figure 11. Lateral view of the velocity field in the mixing and expanded sludge bed sections for
369 the Newtonian fluid simulation

Dead volume of mixing and expanded sludge bed sections for the Newtonian fluid simulation are shown in Figure 12. Obviously, the axial circulation (discussed in Figure 11) has prevented the formation of dead zones near the internal circulation pipe, compared with dead volumes shown in Figure 10a. Figure 12b illustrates the dead zones in the mixing section for the Newtonian fluid simulation. Although the dead zones in the case of Newtonian fluid are smaller than in the non-Newtonian case, a large dead zone still can be detected in the middle of this section, resulting in poor agitation and inefficient pumping flow in the sludge bed section.

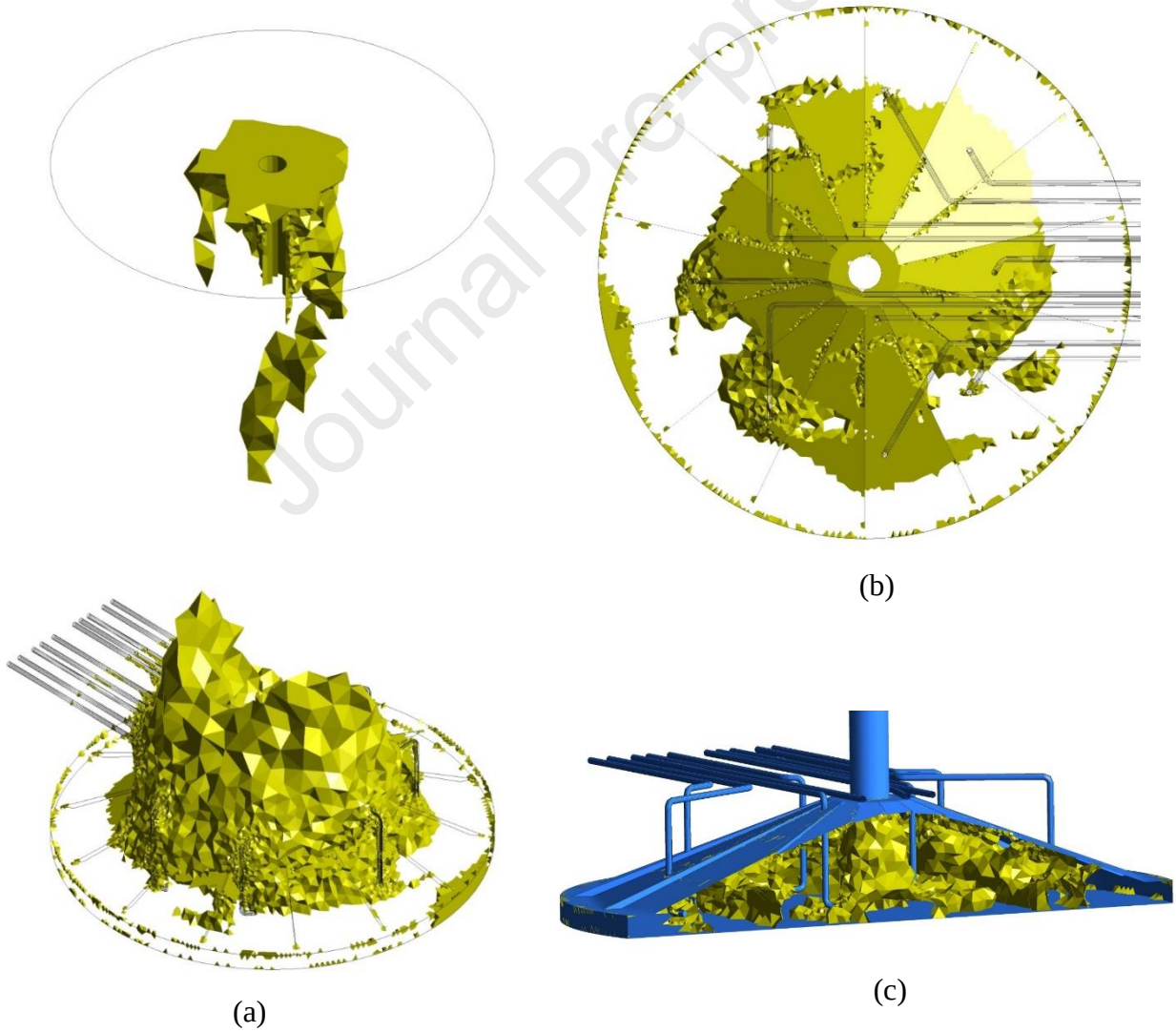

(a) (b) (c)

Figure 12. Dead zones in Newtonian simulation: (a) Mixing and expanded sludge bed sections (b) Mixing section from above (c) A slice of the mixing section

As mentioned earlier, the dead zone is considered as the volume that has a velocity less than 5% of the maximum fluid velocity in the system [35, 45], which can be produced by deficient agitation or vortices. Volume fractions of the dead zones in the mixing and expanded sludge bed sections are given in Table 5 for both Newtonian and non-Newtonian fluids. These values are calculated by measuring the volume of the dead zones detected by the above-mentioned definition. From this table, it can be concluded that more dead zones are formed when the fluid is of non-Newtonian characteristics rather than Newtonian. Therefore, it can be concluded an increasing solid content of the sludge will increase the dead zone fraction in the reactor. The main reason for the formation of these dead zones can be summarized in the rheological properties of the fluid, especially the yield stress and the viscoelastic nature of the fluid, thus, the inefficient upward pumping flow of the mixing section. Note that these results are based on the assumptions undertaken for simulations in specific framework of this study. The flow pattern can change under different flow conditions, thus it is beneficial to investigate the flow patterns in different scenarios (various solid content, different flowrates, etc.).

Table 5. Volume percentage of dead zones in mixing and expanded sludge bed sections

Section	Newtonian	non-Newtonian
Mixing	**45.78%**	**49.34%**
Expanded sludge bed	**4.25 %**	**10.56%**

3.3. Residence Time Distribution

A tracer injection as a pulse through the influent pipes was simulated and its concentration was monitored at the outlet of the expanded sludge bed section. The normalized residence time distributions determined by the tracer method for both types of fluid are shown in Figure 13. The presence of a long tail for both simulations is a sign of dead zones in which the tracer diffuses slowly through the reactor [47]. In the Newtonian case, a small hump can be observed in the RTD. This hump has occurred due to the axial circulation flow in addition to the flow from the internal circulation pipe as discussed in the Newtonian fluid simulation results and presented in Figures 7 and 11.

A small initial time-lag in both curves is a result of an ideal plug flow configuration in the initial part of curves which results in a delay in the exit-age function. Overall, both curves can be represented by combinations of ideal plug flow reactors (PFR), continuous stirred-tank reactors (CSTR) and dead volumes. The volume of the ideal PFR can be calculated considering the time lag and influent rate. The volume of CSTRs can be predicted based on compartment models and the number of CSTRs can be suggested by the serial tanks model [42]. The total reactor mean residence time, ideal plug flow volumes, ideal CSTR volumes (sum of the two reactors in increasing-size CSTRs), dead volumes, *N* values for the tank in series model, *D*/*uL* for the dispersion model and dimensionless variance ($\sigma_\theta{}^2$) for each simulation are shown in Table 6.

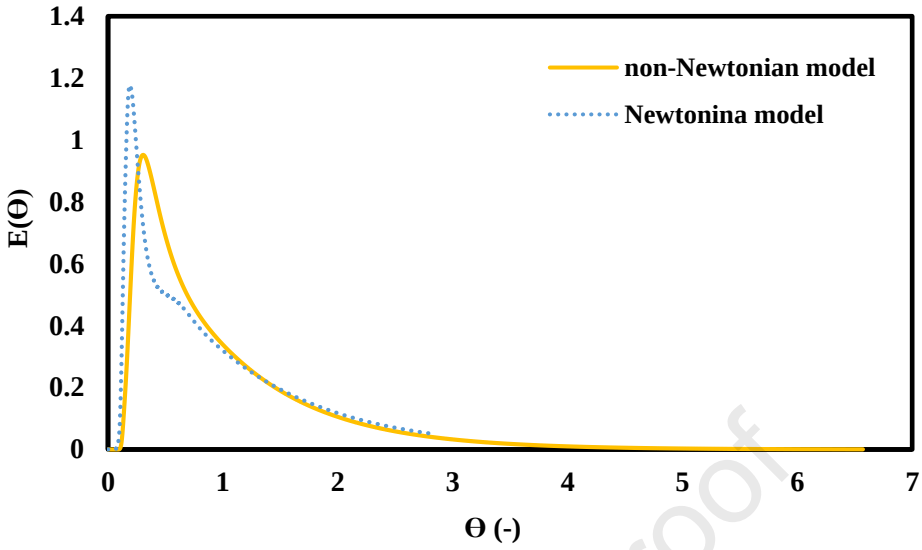

418

419 Figure 13. Exit function curves for Newtonian and non-Newtonian simulations

420

421 Table 6. RTD evaluation results and multi-scale modeling parameters

Simulation	Mean residence time (hr)	Plug flow volume (m^3)	Ideal CSTR volume (m^3)	Dead volume (m^3)	dimensionless variance σ_θ^2	N
Non-Newtonian	2.563	181.683	853.272	149.625	0.709	1.41
Newtonian	2.227	122.100	988.511	73.969	0.702268	1.42

422

423 As stated above, CFD simulation can determine the non-ideality of flow and reveal the dead zones.
424 These simulations can be used for enhancing the mixing process and optimizing the input power.
425 However, calculation time is a limiting factor in this study. Reaching the steady state condition
426 needed 4 to 21 days for different cases. This issue would be more critical if adding the required
427 time for forming the initial flow pattern within the reactor. Also, incorporation of kinetics of the
428 anaerobic digestion demands different and multiple case studies and a sensitivity analysis which
429 will make further investigations more time demanding. This study was focused only on simulating
430 a half of the reactor and for full-size multiphase simulations, runtime will exceedingly increase.
431 Dapelo et al. [28] took the first step toward solving this issue by using a pioneering Lattice-

Boltzmann model for simulating digesters and decreasing the simulation time by removing Euler-Lagrange finite volume CFD constraints and increasing calculation expenses efficiency. However, two-step simulations can be considered as an alternative solution. Incorporating the kinetics of biological process with mathematical models can be used instead of adding different components in CFD simulations and increasing the calculation expenses, especially in regular CFD investigations.

In the present work, different mathematical models were analyzed and compared with CFD results. However, the equal-sized CSTRs model was not evaluated because N (number of CSTRs, Table 4) is not an integer. Therefore, the extended equal-sized CSTRs and increasing-size CSTRs models were used instead. Figure 14 shows the performance of these models against the CFD results. The performance of the EESC model seems to be inaccurate in comparison with the ISC model. The ISC model contains two CSTRs with 1:6 volumetric ratio and represents an acceptable match with the CFD results. The first CSTR is 121.89 m^3 and the second one is 731.37 m^3. These volumes were calculated by fitting the model exit-age function to the CFD results and considering the proposed CSRT volume in Table 6. Figure 14 also demonstrates the performance of the proposed compartment model. This model contains a plug flow reactor in addition to the ISC model, which adds a time lag in the exit-age function. It can be seen in this figure that this model fits better to the CFD results. The schematic of this model is presented in Figure 4. In fact, the increasing-size CSTRs model considers the same volume as the ISC model. Both compartment model and ISC model can be equally considered for integration of kinetics.

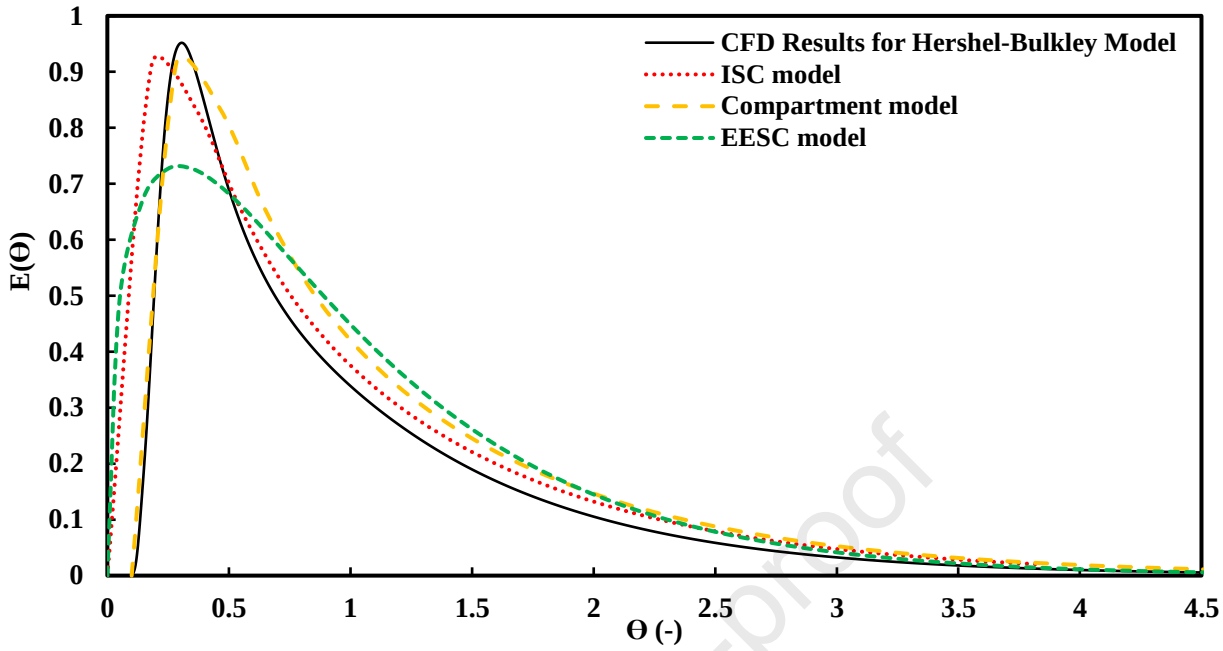

Figure 14. Performance of ISC, EESC and compartment models against CFD simulations

4. Conclusions

This study evaluated the mixing of an anaerobic digestion reactor by observing converged simulated flow patterns, dead zone evaluation, and RTD analysis. It was found that there are noticeable dead zones in the reactor, which covers 49.3 volume percent of the mixing section and 10.6 volume percent of the expanded sludge bed section volume. The formation of these dead zones can be attributed to the rheological properties of the fluid in addition to the inefficient mixing and lack of flow pumping within the reactor. Also, insufficient mixing of influents with the circulated flow makes the internal circulation ineffective. Therefore, modifications, such as rearranging the influent pipes (injection direction), adding baffles, mixing section reconfiguration, etc., can be considered to enhance the mixing efficiency.

Dead zones result in a non-ideal flow pattern in the reactor, which was described with a compartment model consisting of a 181.6 m^3 plug flow reactor, 149.6 m^3 dead zone, 853.2 m^3 ideally mixed reactor and a recycle flow. Increasing-size CSTRs and compartment models described this flow pattern acceptably and their performance compared with CFD results. It is also shown that an increase in the solid content of the influent results in non-Newtonian behavior, which causes more deviation from the ideal well-mixed reactor to plug flow reactor and also the formation of larger dead zones. Extended equal-sized CSTRs, increasing-size CSTRs and a compartment model were utilized to describe the flow pattern in the reactor. ISC and compartment models showed reasonable performance and can be used for incorporating the kinetics in future studies.

Acknowledgements

The authors wish to thank Kasper Kjellberg (Senior Technology Manager, Novozymes) who kindly provided the geometry dimensions and process details. The authors also gratefully acknowledge the Technical University of Denmark for the partial support of this study.

Nomenclature

AD Anaerobic Digestion

ADM1 Anaerobic digestion model No. 1

CFD Computational Fluid Dynamics

$D_{i,m}$ Mass diffusion coefficient for species i (m^2s^{-1})

D_t Turbulent diffusivity (m^2s^{-1})

$E(t)$ Exit-age function (s)

ESC Equal-sized CSTRs

EESC Extended equal-sized CSTRs

CARPT Computer Automated Radioactive Particle Tracking

CT Computed Tomography

PEPT Positron Emission Particle Tracking

GCI Grid Convergence Index

G_b Turbulence kinetic energy generation by buoyancy

G_k Turbulence kinetic energy generation by velocity gradients

IC Internal Circulation

ISC Increasing-size CSTRs

K Consistency coefficient (Pa s^n)

k Turbulent kinetic energy (m^2s^{-2})

n Power law index

N Number of CSTR tanks

p Static pressure (Pa)

RTD Residence Time Distribution

S_{Ct} Turbulent Schmidt number

TSS Total Suspended Solids (kgm^{-3})

$\bar{t}$ Mean residence time (s)

UASB Upflow Anaerobic Sludge Blanket

$\vec{u}$ Absolute velocity (m s^{-1})

Greek letters

513 μ_t Turbulent viscosity (m^2s^{-1})

514 ε Rate of dissipation (m^2s^{-3})

515 ρ Density (kg m^{-3})

516 σ_k k Prandtl number

517 σ_ε ε Prandtl number

518 σ_t^2 Distribution variance of the RTD

519 σ_θ^2 Dimensionless variance of the RTD

520 τ Shear stress (N m^{-2})

521 θ Normalized time (-)

522

523 ## References

524 [1] Tumilar A, Sharma M, Milani D, Abbas A. Modeling and Simulation Environments for
525 Sustainable Low-Carbon Energy Production–A Review. Chemical Product and Process
526 Modeling. 2016;11(2):97-124.

527 [2] Batstone DJ, Keller J, Angelidaki I, Kalyuzhnyi S, Pavlostathis S, Rozzi A, et al. The IWA
528 anaerobic digestion model no 1 (ADM1). Water Science and technology. 2002;45(10):65-
529 73.

530 [3] Astals S, Esteban-Gutiérrez M, Fernández-Arévalo T, Aymerich E, García-Heras J, Mata-
531 Alvarez J. Anaerobic digestion of seven different sewage sludges: a biodegradability and
532 modelling study. Water research. 2013;47(16):6033-43.

533 [4] Souza TS, Carvajal A, Donoso-Bravo A, Peña M, Fdz-Polanco F. ADM1 calibration using
534 BMP tests for modeling the effect of autohydrolysis pretreatment on the performance of
535 continuous sludge digesters. Water research. 2013;47(9):3244-54.

[5] Batstone DJ, Keller J. Industrial applications of the IWA anaerobic digestion model No. 1 (ADM1). Water Science and Technology. 2003;47(12):199-206.

[6] Batstone D, Tait S, Starrenburg D. Estimation of hydrolysis parameters in full-scale anerobic digesters. Biotechnology and bioengineering. 2009;102(5):1513-20.

[7] Baudez J, Slatter P, Eshtiaghi N. The impact of temperature on the rheological behaviour of anaerobic digested sludge. Chemical Engineering Journal. 2013;215:182-7.

[8] Wu B. Advances in the use of CFD to characterize, design and optimize bioenergy systems. Computers and Electronics in Agriculture. 2013;93:195-208.

[9] López I, Borzacconi L. UASB reactor hydrodynamics: residence time distribution and proposed modelling tools. Environmental technology. 2010;31(6):591-600.

[10] Lindmark J, Thorin E, Fdhila RB, Dahlquist E. Effects of mixing on the result of anaerobic digestion. Renewable and Sustainable Energy Reviews. 2014;40:1030-47.

[11] Leonzio G. Study of mixing systems and geometric configurations for anaerobic digesters using CFD analysis. Renewable energy. 2018;123:578-89.

[12] Gerardi MH. The microbiology of anaerobic digesters: John Wiley & Sons; 2003.

[13] Dapelo D, Bridgeman J. Assessment of mixing quality in full-scale, biogas-mixed anaerobic digestion using CFD. Bioresource technology. 2018;265:480-9.

[14] Dapelo D, Alberini F, Bridgeman J. Euler-Lagrange CFD modelling of unconfined gas mixing in anaerobic digestion. Water research. 2015;85:497-511.

[15] Monteith HD, Stephenson JP. Mixing efficiencies in full-scale anaerobic digesters by tracer methods. Journal (Water Pollution Control Federation). 1981:78-84.

[16] Karim K, Varma R, Vesvikar M, Al-Dahhan M. Flow pattern visualization of a simulated digester. Water Research. 2004;38(17):3659-70.

559 [17] Sindall RC, Dapelo D, Leadbeater T, Bridgeman J. Positron emission particle tracking
560 (PEPT): A novel approach to flow visualisation in lab-scale anaerobic digesters. Flow
561 Measurement and Instrumentation. 2017;54:250-64.
562 [18] Maßmann T, Kocks C, Parakenings L, Weber B, Jupke A. Two-Dimensional CFD based
563 Compartment Modeling for Dynamic Simulation of Semi-batch Crystallization Processes
564 in Stirred Tank Reactors. Computers & Chemical Engineering. 2020:106933.
565 [19] Elqotbi M, Vlaev S, Montastruc L, Nikov I. CFD modelling of two-phase stirred
566 bioreaction systems by segregated solution of the Euler–Euler model. Computers &
567 Chemical Engineering. 2013;48:113-20.
568 [20] Michalopoulos I, Kamperidis T, Seintis G, Pashos G, Lytras C, Papadopoulou K, et al.
569 Experimental and numerical assessment of the hydraulic behavior of a pilot-scale Periodic
570 Anaerobic Baffled Reactor (PABR). Computers & Chemical Engineering. 2018;111:278-
571 87.
572 [21] Karama A, Onyejekwe O, Brouckaert C, Buckley C. The use of computational fluid
573 dynamics (CFD). Technique for evaluating the efficiency of an activated sludge reactor.
574 Water science and technology. 1999;39(10-11):329-32.
575 [22] Hague J, Ta C, Biggs M, Sattary J. Small scale model for CFD validation in DAF
576 application. Water science and technology. 2001;43(8):167-73.
577 [23] Peplinski DK, Ducoste JJ. Modeling of disinfection contactor hydraulics under uncertainty.
578 Journal of Environmental Engineering. 2002;128(11):1056-67.
579 [24] Liu J, Crapper M, McConnachie G. An accurate approach to the design of channel
580 hydraulic flocculators. Water research. 2004;38(4):875-86.

[25] Meister M, Rezavand M, Ebner C, Pümpel T, Rauch W. Mixing non-Newtonian flows in anaerobic digesters by impellers and pumped recirculation. Advances in Engineering Software. 2018;115:194-203.

[26] López-Jiménez PA, Escudero-González J, Martínez TM, Montanana VF, Gualtieri C. Application of CFD methods to an anaerobic digester: The case of Ontinyent WWTP, Valencia, Spain. Journal of Water Process Engineering. 2015;7:131-40.

[27] Wu B. Integration of mixing, heat transfer, and biochemical reaction kinetics in anaerobic methane fermentation. Biotechnology and bioengineering. 2012;109(11):2864-74.

[28] Dapelo D, Trunk R, Krause MJ, Bridgeman J. Towards Lattice-Boltzmann modelling of unconfined gas mixing in anaerobic digestion. Computers & Fluids. 2019;180:11-21.

[29] Huang Y, Ma Y, Wan J, Wang Y. Mathematical modelling of the internal circulation anaerobic reactor by Anaerobic Digestion Model No. 1, simultaneously combined with hydrodynamics. Scientific reports. 2019;9(1):6249.

[30] Dapelo D, Bridgeman J. Euler-Lagrange Computational Fluid Dynamics simulation of a full-scale unconfined anaerobic digester for wastewater sludge treatment. Advances in Engineering Software. 2018;117:153-69.

[31] Wu B. CFD investigation of turbulence models for mechanical agitation of non-Newtonian fluids in anaerobic digesters. Water research. 2011;45(5):2082-94.

[32] Vakili M, Esfahany MN. CFD analysis of turbulence in a baffled stirred tank, a three-compartment model. Chemical Engineering Science. 2009;64(2):351-62.

[33] Kukuková A, Moštěk M, Jahoda M, Machoň V. CFD prediction of flow and homogenization in a stirred vessel: Part I vessel with one and two impellers. Chemical

Engineering & Technology: Industrial Chemistry-Plant Equipment-Process Engineering-Biotechnology. 2005;28(10):1125-33.

[34] ANSYS IAFUsG, Release 17.2.

[35] Vesvikar MS, Al-Dahhan M. Flow pattern visualization in a mimic anaerobic digester using CFD. Biotechnology and Bioengineering. 2005;89(6):719-32.

[36] Karim K, Thoma GJ, Al-Dahhan MH. Gas-lift digester configuration effects on mixing effectiveness. Water research. 2007;41(14):3051-60.

[37] Craig K, Nieuwoudt M, Niemand LJ. CFD simulation of anaerobic digester with variable sewage sludge rheology. Water research. 2013;47(13):4485-97.

[38] Hurtado F, Kaiser A, Zamora B. Fluid dynamic analysis of a continuous stirred tank reactor for technical optimization of wastewater digestion. Water research. 2015;71:282-93.

[39] Bridgeman J. Computational fluid dynamics modelling of sewage sludge mixing in an anaerobic digester. Advances in Engineering Software. 2012;44(1):54-62.

[40] Feldman H, Flores-Alsina X, Kjellberg K, Jeppsson U, Batstone DJ, Gernaey KV. Model-based analysis and optimization of a full-scale industrial high-rate anaerobic bioreactor. Biotechnology and bioengineering. 2018;115(11):2726-39.

[41] Landry H, Laguë C, Roberge M. Physical and rheological properties of manure products. Applied Engineering in Agriculture. 2004;20(3):277.

[42] Levenspiel O. Chemical reaction engineering. Industrial & engineering chemistry research. 1999;38(11):4140-3.

[43] Qi W-K, Guo Y-L, Xue M, Li Y-Y. Hydraulic analysis of an upflow sand filter: tracer experiments, mathematical model and CFD computation. Chemical engineering science. 2013;104:460-72.

626 [44] Roache PJ. Verification and validation in computational science and engineering: Hermosa
627 Albuquerque, NM; 1998.
628 [45] Terashima M, Goel R, Komatsu K, Yasui H, Takahashi H, Li Y, et al. CFD simulation of
629 mixing in anaerobic digesters. Bioresource technology. 2009;100(7):2228-33.
630 [46] Golshan S, Zarghami R, Norouzi HR, Mostoufi N. Granular mixing in nauta blenders.
631 Powder Technology. 2017;305:279-88.
632 [47] Fogler HS. Elements of Chemical Reaction Engineering: Pearson Higher Education &
633 Professional Group; 2013.

Declaration of interests

☒ The authors declare that they have no known competing financial interests or personal relationships that could have appeared to influence the work reported in this paper.

☐The authors declare the following financial interests/personal relationships which may be considered as potential competing interests: